# Development of a Kinematic 3D Carpal Model to Analyze In Vivo Soft-Tissue Interaction Across Multiple Static Postures

G. Elisabeta Marai, Joseph J. Crisco and David H. Laidlaw

*Abstract*— We developed a subject-specific kinematic model to analyze *in vivo* soft-tissue interaction in the carpus in static, unloaded postures. The bone geometry was extracted from a reference computed tomography volume image. The soft-tissue geometry, including cartilage and ligament tissues, was computationally modeled based on kinematic constraints; the constraints were extracted from multiple computed tomography scans corresponding to different carpal postures. The data collected *in vivo* was next coupled with numerical simulation in order to analyze the role of soft-tissues in different postures. The resulting model extends the state of biomecanical modeling by incorporating soft-tissue constraints across the carpus range of motion, while successfully using only physiological constraints. The model results suggest that soft-tissue wrapping constraints have substantial impact on carpus stability.

## I. INTRODUCTION

The carpal bones of the wrist and their cartilage and supporting ligaments are frequently prone to injuries, including repetitive strain injuries and osteoarthritis, due to their small size and high levels of use. How do these injuries occur, and why do certain therapies work only for certain individuals? Subject-specific, computational models of the carpus can help answer such questions.

However, developing computational models of the carpus poses significant challenges. For example, due to their small size, many of the inputs we need to build functional models of the carpus — such as individual wrist ligaments and their rest-length — are currently not measurable in live individuals. Another challenge is deciding what level of modeling detail is necessary in order to generate biologically significant measurements, while keeping the resulting models efficient to simulate.

Numerous methods have been developed for the study of articulation biomechanics, ranging from cadaveric to computational studies. Nevertheless, the wrist joint, consisting of eight carpal bones positioned between the two bones of the forearm and the five metacarpal bones of the hand, has proven difficult to model computationally due to the number of bodies involved and complexity of the soft tissue interaction. Multibody contact analyses of the wrist joint have long been limited to two-dimensional studies using non-physiologic constraint parameters [1], [2]. A three-dimensional (3D) computational approach to modeling carpal

joints has also been developed [3]. In this approach, 3D solid finite element meshes representing the bones were hollowed by eliminating all elements that did not reach the external mesh surface in order to reduce the number of nodes and elements in the mesh, and thereby improve model efficiency. The articulated bony surfaces were extruded to mimic cartilage. Several pairs of bones were fused into single rigid bodies, ligaments were modeled as line springs, and only one static posture was modeled. Nevertheless, in this model the bone motion also had to be restricted artificially through non-physiological constraints in order to prevent the wrist from collapsing when loads were applied.

In order to improve upon existing results and avoid non-physiological constraints, new methods of modeling the wrist are necessary. We propose a hybrid modeling approach that couples directly measured bone geometry with computational models of soft-tissues. The method uses as input medical volume images of the joint bones, kinematic measurements and expert anatomical knowledge, and builds from these data a 3D model of the carpus. The data obtained *in vivo* through medical imaging is then coupled with numerical simulation to analyze the role of soft-tissues in the functioning of the joint.

## II. METHODS

### A. Data Acquisition

The wrist bones of a male volunteer were repeatedly imaged through computed tomography (CT) using a GE Hispeed Advantage scanner with scan parameters 80kV, 80mA and image resolution 0.94 x 0.94 x 1 mm$^3$. Seven volume images corresponding to seven distinct postures were acquired within the full range of motion of the wrist. Four of the targeted wrist positions were: $40^o$ of flexion, $40^o$ extension, $30^o$ of ulnar deviation, and $10^o$ of radial deviation. The remaining positions were combinations of these initial in-plane motions (e.g., $40^o$ of flexion with $30^o$ of ulnar deviation). These multiple postures allow us to model the soft-tissue geometry and kinematic constraints across the range of motion, as described in section II-B. An additional higher-resolution scan (0.31 x 0.31 x 1 mm$^3$) was acquired in a reference neutral posture, allowing us to segment the bone surfaces with higher accuracy.

The bone surfaces corresponding to the eight carpal bones, the two forearm bones, and the five metacarpal bones were next segmented and modeled as triangular meshes from the neutral posture scan [5]. Finally, each bone surface was registered accurately through the sequence of remaining CT volume images [6]. The registration procedure reported the
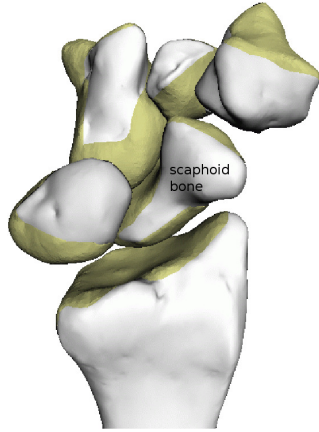
Fig. 1. Palmar view of a six-bone subset of the human wrist showcasing the bones (white) and articular cartilage (yellow) interacting directly with the scaphoid bone (data courtesy of Primal Pictures). This structure includes nine pairwise articulations and fifteen ligaments that may impact scaphoid kinematics and presents a predictive modeling opportunity: no muscles insert on the scaphoid bone. Scaphoid motion is defined solely by bone shapes, bony articulations, and ligaments.

relative motion of each bone from one articulation posture to another.

### B. Model Construction

The model we built includes three-dimensional geometric data of the eight carpal bones, two forearm bones, and five metacarpals, nine pairwise cartilage articulations, and fifteen ligaments that may affect the kinematics of the scaphoid bone (Fig. 1). The scaphoid bone and its surrounding articulations are of significant clinical interest: the bone is frequently subject to fractures, and its connecting ligaments are often subject to tears and surgical intervention. Notably, there are no muscle insertions on the scaphoid bone. This lack of muscle insertions provides an excellent modeling opportunity: we can study scaphoid kinematics without having to specify external muscle forces.

Cartilage maps were reconstructed based on the minimum inter-bone distance across the individual postures (see [7] for full details). Summarizing this reference, the base bone surface mesh was offset for each bone surface involved in a given articulation in the direction of the surface normal to produce "just touching" tissue thickness across the range of motion; the resulting cartilage maps are further modeled as an incompressible, deformable height field and calibrated against anatomy-book data.

We generated ligament fiber paths for 15 ligament bundles, as follows. We manually identified ligament insertion sites based on anatomical expert knowledge. We defined three to four equally spaced fibers per ligament bundle to account for the band-like structure of ligaments. For each fiber and joint pose, we automatically generated minimum-length paths constrained to avoid bone penetration (see [4] for full details). An example ligament fiber interacting with multiple bones is shown in Fig. 2. For each ligament fiber
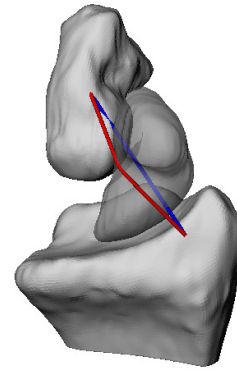


Fig. 2. Ligament fiber interacting with multiple bones. The computed minimum-length path is shown in red, the straight line between the two insertion sites is shown in blue. Note the significant deflection of the generated path from the straight line.

we computed the minimum path length. The resulting fiber paths were visually validated against the anatomy-book data.

### C. Numerical Simulation

Cartilage maps were modeled and simulated as incompressible, deformable height fields. The resulting contact was validated against *in vitro* data [7]. The description of deformable articular contact is based on the simplified theory of contact from Blankevoort et al. [8] for thin layers of isotropic, linear-elastic material bonded to a rigid foundation. The material properties of the cartilage on two bodies in contact are assumed to be equal. The simplified contact description is a first-order approximation of the relation between the normal surface stress $\sigma_n$ and the surface displacement $u_n$ normalized by the surface thickness $t_n$:

$$\sigma_n = S(u_n/t_n) \qquad (1)$$

with

$$S = \frac{(1-\nu)E}{(1+\nu)(1-2\nu)} \qquad (2)$$

where $E$ is the elastic modulus and $\nu$ is Poisson's ratio. This description of articular contact deformation is strictly linear and will only be valid for small surface displacements.

The compressive cartilage contact force and moment are evaluated by integration of the contact stresses over the surface $\Omega$:

$$\mathrm{f}_{cartilage} = -\int\int_{\Omega} \sigma_n \mathrm{n}\ d\Omega \qquad (3)$$

$$\mathrm{m}_{cartilage} = -\int\int_{\Omega} \sigma_n \mathrm{c} \times \mathrm{n}\ d\Omega \qquad (4)$$

where c is the relative position vector of the cartilage contact with respect to the center of mass, and n the direction of the normal.

Ligaments were simulated as collections of elastic fibers characterized by their rest length and elasticity coefficient. Invasive studies on the human knee show that ligaments tear when stretched above 10% of their rest length [9]. Extrapolating to the wrist, and considering that the range of motion we use as input was unlikely to stretch ligaments

to their maximum length, we estimated the fiber rest length should be around 95% of the computed maximum length. We considered a ligament to be lax in the postures in which its functional length was less than its estimated rest length.

Ligament contact forces and moments were computed separately for ligament-bone contact due to ligament insertions and ligament-bone contact due to ligament wrapping. Let $m$ be the total number of ligament fibers modeled, and $o_j$ the number of insertions for ligament $j$. The ligament insertion contact force and moment were computed following Blankevoort et al.[8] as:

$$f_{lig.ins.} = \sum_{j=1}^{m} \sum_{i=1}^{o_j} K_{lig} \left( \frac{l_j - l_{j_0}}{l_{j_0}} \right)^2 v_{ji} \qquad (5)$$

$$m_{lig.ins.} = \sum_{j=1}^{m} \sum_{i=1}^{o_j} s_{ji} \times f_{\text{lig.ins.}\, ji} \qquad (6)$$

where $l_{j_0}$ is the rest length of ligament $j$, $v_{ji}$ is the ligament direction at the insertion site $i$, and $s_{ji}$ the relative position vector of the ligament insertion with respect to the center of mass.

Similarly, the ligament wrapping contact force and moment are computed as:

$$f_{lig.wrap} = \sum_{j=1}^{m} \sum_{i=1}^{n_j} K_{lig} \left( \frac{l_j - l_{j_0}}{l_{j_0}} \right)^2 \alpha_{ij} p_{ji} \qquad (7)$$

$$m_{lig.wrap} = \sum_{j=1}^{m} \sum_{i=1}^{n_j} s_{ji} \times f_{\text{lig.wrap}\, ji} \qquad (8)$$

where $n_j$ is the number of points at which ligament $j$ contacts the bone surface through wrapping, $l_{j_0}$ is the rest length of ligament $j$, $p_{ji}$ is the sum of the ligament directions left and right of the contact point $i$, $\alpha_{ij}$ sums the projections of the left and right ligament directions in the $p_{ji}$ direction (i.e., the directional sum of forces passing on either side of the point), and $s_{ji}$ is the relative position vector of the ligament contact point with respect to the center of mass.

We used *in vitro* determined values for $S_{cart}$, the cartilage stiffness parameter, $K_{lig}$, the ligament elasticity coefficient, and the scaphoid mass (Table I) [10], [11]. In the absence of stiffness and elasticity constants for the human wrist, material parameters representative of the human knee were used for the wrist cartilage and ligaments. All ligaments were assumed to have the same elasticity coefficient.

Because each volume image of the joint is acquired in a quasi-static posture, the net force and moment acting on a bone at each pose are:

$$f_{net} = f_{cartilage} + f_{lig.ins.} + f_{lig.wrap} + f_{external} \qquad (9)$$

$$m_{net} = m_{cartilage} + m_{lig.ins.} + m_{lig.wrap} + m_{external} \qquad (10)$$

where $f_{external}$ and $m_{external}$ are the external force and momentum.

Because there are no muscle insertions on the scaphoid bone, at each posture the values of $f_{cartilage} + f_{lig.ins.} + f_{lig.wrap}$ and $m_{cartilage} + m_{lig.ins.} + m_{lig.wrap}$ resulting for the scaphoid

TABLE I
MATERIAL PROPERTIES USED WHEN SIMULATING THE WRIST JOINT

| parameter | value |
|---|---|
| $S_{cart}$ | $4MPa$ |
| $K_{lig}$ | $10^6 N/m^2$ |
| Scaphoid mass | $3g$ |

bone when using the parameters in Table I should be reasonably small — the same order of magnitude with the gravity on the scaphoid bone. We use this $(f_{net}, m_{net})$ balance observation to validate the parameter values in Table I.

As in Carrigan et al. [3], in our simulations all the bones except for the scaphoid bone were fixed; the scaphoid bone was free to move under the influence of contact forces and gravity. We used the explicit forward Euler method to integrate the scaphoid state through time (0.01s time-step), and the penalty-method (0.005 penalty factor) to resolve inter-penetrations. Articular contact was rigidly approximated whenever cartilage deformation was under 5%, since such small deformations result in negligible deviations in the surface shape (0.007mm to 0.035mm), in particular in comparison to the size of the bones and the bounds of experimental error. Ligaments were allowed to deform up to 10% of their estimated rest-length. After this threshold, ligament-bone contact was treated as rigid.

## III. EXPERIMENTAL RESULTS

The goal of the experiments described in this section was to clarify the role played by ligaments in stabilizing the scaphoid bone. To this end, we first validated the *in vitro* parameter values in Table I by evaluating $(f_{net}, m_{net})$ at each joint posture. The resulting values (0.15N $\pm$ 0.09N force, 0.74Nm $\pm$ 0.51Nm torque) were reasonably small, comparable with the gravity on the scaphoid bone (0.03N, 0Nm).

Next, we simulated the motion of the scaphoid bone when the start conditions were given by the neutral posture. All bones except the scaphoid were fixed and ligament-related constraints were not taken into account. In each simulation the scaphoid remained stable, inside the six-bone subset joint of Fig. 1. For each simulation we report the total helical axis motion — translation and rotation — of the scaphoid bone. The total scaphoid motion when the gravitational force pushed the scaphoid bone towards the dorsal side of the joint was (-0.56mm, 1.41°). The total motion when the gravitational force pushed the scaphoid bone outside the joint — towards the palmar side — was (1.41mm, 1.45°). The simulations were stopped after 6s simulated time. These results indicate that in the neutral pose the scaphoid bone is locked in place by the surrounding bones.

Next, we simulated the motion of the scaphoid bone when the start conditions were given by an extended pose. All bones except the scaphoid bone were fixed. Initially, ligament-related constraints were not taken into account. The total scaphoid motion when the gravitational force pushed the scaphoid bone towards the dorsal side of the joint was (-0.07mm, 3.16°); the bone remained inside the joint. When

the gravitational force pushed the bone outside the joint — towards the palmar side, the scaphoid dislocated from the joint and continued to slide away from the joint, in the direction of the gravitational force. The simulation was stopped after 15s. The total recorded scaphoid motion was (-5.28mm, $-2.45°$).

We repeated the extended-pose dislocation experiment, this time taking into account ligament-related constraints. At the start of the simulation, we recorded five active ligament bundles. As the simulation progressed, three of these ligaments were stretched to the maximum length, two became inactive, and one additional ligament was activated. Notably, two of the maximally-stretched ligaments wrap around the scaphoid bone: the radio-scapho-capitate ligament and the palmar mid-carpal scaphoid ligament. The constraints imposed by ligament-bone contact through ligament insertion points and wrapping points were sufficient to prevent the scaphoid from becoming dislocated from the six-bone subset joint. The simulation was stopped after 6s; the total recorded motion was (-0.99mm, $-2.45°$).

Each simulation was computed in under 2 minutes on an AMD Athlon 64 X2 processor, 2 GHz.

## IV. DISCUSSION AND CONCLUSION

This study has successfully coupled data obtained *in vivo* with numerical simulation to develop a predictive tool for understanding the role of soft-tissues in the functioning of the wrist joint. In particular, our results show that wrist ligaments play an important role in stabilizing the joint. We note that our results are consistent with earlier studies on scaphoid motion [3], in which, in the absence of ligament wrapping, the scaphoid motion had to be artificially constrained to a plane to avoid joint collapse.

We used several modeling simplifications in our approach. Our models do not include the top layers of a joint — muscles, the neurovascular system, fat and skin. Ligament interconnectivity is not modeled, nor are the synovial sac and fluid. We approximate the viscoelastic properties of ligaments and cartilage. Bones are approximated as rigid bodies and bone-mass is assumed to be uniformly distributed. The models we generate could be enriched by considering intrinsic and extrinsic factors such as soft tissue composition, bone tissue composition, muscle forces, and joint compression. We further extrapolate knee *in vitro* knowledge to the wrist when we assume that ligaments tear when stretched above 10% of their rest length; the 10% threshold may not be correct. We also assume that wrist ligaments are characterized by the same elasticity coefficient. When more data about the elastic properties of wrist ligaments becomes available, our carpus model may need to be updated.

Our simulation uses the forward Euler integration method and the penalty-method contact model. More intricate techniques exist; such techniques involve subdividing time to find the exact moment of collisions and then applying impulses or resting forces as needed. Such methods provide in general more accuracy and stability, although simulation stability has not been an issue in our experiments so far.

In conclusion, we presented a medical-image based method for constructing and simulating carpal joint models. The method uses as input medical volume images of the joint bones, articulation kinematics, and *in vitro* knowledge. The models we generate can help clarify the role of soft-tissue interaction in the kinetic response of the joint.

The results presented prove it is possible to couple *in vivo* data with numerical simulation to understand the role of soft-tissues in the functioning of the wrist joint, while avoiding non-physiological constraints. Only one bone was allowed to move freely in our experiments, while the other bones were fixed. A natural next step is to apply the actual kinematics to some of the bones in the model and concentrate predictive efforts on one bone at a time. Future studies may also couple finite element analysis with our kinematic carpus model.

### REFERENCES

[1] Anderson, D. D., and T. E. Daniel. A contact-coupled finite element analysis of the radiocarpal joint. Semin. Arthro. 6:30-36, 1995.
[2] Oda, M., H. Hashizume, T. Miyake, H. Inoue, and N. Nagayama. A stress distribution analysis of a ceramic lunate replacement for Kienbocks disease. J. Hand Surg. 25B:492- 498, 2000.
[3] Carrigan, S.D., Whiteside, R.A., Pichora, D.R., and Small, C.F., Development of a Three-Dimensional Finite Element Model for Carpal Load Transmission in a Static Neutral Posture, Annals of Biomed. Eng., Vol 31, pages 718-725, 2003.
[4] Marai, G.E., Laidlaw, D.H., Demiralp, C., Andrews, S., Grimm, C.M., Crisco, J.J., Estimating joint contact areas and ligament lengths from bone kinematics and surfaces, IEEE Trans. on Biomedical Engineering, 51(5), pages 790-799, 2003.
[5] Crisco, J.J., McGovern, R.D. Wolfe, S.W., A non-invasive technique for measuring in vivo three-dimensional carpal bone kinematics, J. Orthopaedic Research, 17(1), pages 96–100, 1999.
[6] Marai, G.E., Laidlaw, D.H. and Crisco, J.J., Super-Resolution Registration Using Tissue-Classified Distance Fields. IEEE Trans. on Medical Imaging 25(2), pages 177- 187, 2006.
[7] Marai, G.E., Laidlaw, D.H. and Crisco, J.J., A Kinematics-Based Method for Generating Cartilage Maps and Deformations in the Multi-Articulating Wrist Joint From CT Images, IEEE 2006 Conference of the Engineering in Medicine and Biology Society (EMBC'06), pages 2079-2082, 2006.
[8] Blankevoort, L., Kuiper, J. H., Huiskes, R., and Grootenboer, H. J., Articular contact in a three-dimensional model of the knee, J Biomech. Vol. 24, No. 11, pages 1019-1031, 1991.
[9] Frey, M., Riener, R., Michas, C., Regenfelder, F., Burgkart, R., Elastic properties of an intact and ACL-ruptured knee joint: measurement, mathematical modelling, and haptic rendering, J Biomech.39(8):1371-1382, 2006.
[10] Sirkett, D.M., Mullineux, G., Giddins, G.E.B., Miles, A.W. , A Kinematic Model of the Wrist based upon Maximization of Joint Contact Area, Proceedings of the Institution of Mechanical Engineers Part H: The Journal of Engineering in Medicine 218, pages 349-359, 2004.
[11] Thoomukuntla, B.R., Pillai, R.R., McIff, T.E., Bilgen, M., Ateshian, G.A., and Fischer, K.J., Validation of an MRI-Based Method for In Vivo Joint Contact Mechanics Analyses, American Society of Mechanical Engineers Summer Bioengineering Conference, Vail CO, 2005.